JCI insight

RESEARCH ARTICLE

Essential role of $K_{ir}5.1$ channels in renal salt handling and blood pressure control

Oleg Palygin,[1,2] Vladislav Levchenko,[1] Daria V. Ilatovskaya,[1] Tengis S. Pavlov,[1] Oleh M. Pochynyuk,[3] Howard J. Jacob,[1,4] Aron M. Geurts,[1,4,5] Matthew R. Hodges,[1,2] and Alexander Staruschenko[1,5]

[1]Department of Physiology and [2]Neuroscience Research Center, Medical College of Wisconsin, Milwaukee, Wisconsin, USA. [3]Department of Integrative Biology, University of Texas Health Science Center Medical School, Houston, Texas, USA. [4]Human and Molecular Genetics Center and [5]Cardiovascular Center, Medical College of Wisconsin, Milwaukee, Wisconsin, USA.

Supplementing diets with high potassium helps reduce hypertension in humans. Inwardly rectifying K^+ channels $K_{ir}4.1$ (*Kcnj10*) and $K_{ir}5.1$ (*Kcnj16*) are highly expressed in the basolateral membrane of distal renal tubules and contribute to Na^+ reabsorption and K^+ secretion through the direct control of transepithelial voltage. To define the importance of $K_{ir}5.1$ in blood pressure control under conditions of salt-induced hypertension, we generated a *Kcnj16* knockout in Dahl salt-sensitive (SS) rats ($SS^{Kcnj16-/-}$). $SS^{Kcnj16-/-}$ rats exhibited hypokalemia and reduced blood pressure, and when fed a high-salt diet (4% NaCl), experienced 100% mortality within a few days triggered by salt wasting and severe hypokalemia. Electrophysiological recordings of basolateral K^+ channels in the collecting ducts isolated from $SS^{Kcnj16-/-}$ rats revealed activity of only homomeric $K_{ir}4.1$ channels. $K_{ir}4.1$ expression was upregulated in $SS^{Kcnj16-/-}$ rats, but the protein was predominantly localized in the cytosol in $SS^{Kcnj16-/-}$ rats. Benzamil, but not hydrochlorothiazide or furosemide, rescued this phenotype from mortality on a high-salt diet. Supplementation of high-salt diet with increased potassium (2% KCl) prevented mortality in $SS^{Kcnj16-/-}$ rats and prevented or mitigated hypertension in $SS^{Kcnj16-/-}$ or control SS rats, respectively. Our results demonstrate that $K_{ir}5.1$ channels are key regulators of renal salt handling in SS hypertension.

Introduction

It is well recognized that higher levels of sodium intake are associated with elevated blood pressure (1–3). Importantly, the effect of dietary sodium on blood pressure is dependent on other components of the diet and, specifically, its potassium content (2, 4). The large-scale Prospective Urban Rural Epidemiology (PURE) study examined the association of urine sodium and potassium excretion (as surrogates of sodium and potassium intake) with blood pressure in more than 100,000 participants. It was reported that higher estimated potassium excretion was associated with a lower risk of the composite of death and major cardiovascular events (3). In another study, the PURE investigators noted an inverse association between estimated potassium excretion and systolic blood pressure, with each gram increment in estimated potassium excretion per day resulting in a 1.08 mmHg decrease in systolic blood pressure. The highest blood pressures were observed in individuals with the maximum estimated sodium excretion combined with the lowest estimated potassium excretion (2). Similarly, a cluster-randomized, controlled trial, in which participants increased potassium consumption and reduced sodium consumption through the use of potassium-enriched salt, showed a reduction in cardiovascular mortality among those assigned to the higher-potassium group (5). Despite the highly relevant clinical and translational magnitude of these studies, specific mechanisms underlying these beneficial effects of high potassium remain unclear.

The plasma potassium level is maintained within rather narrow limits (between 3.6 and 5 mmol/l) and is tightly controlled by multiple mechanisms (6, 7). The kidneys are central in controlling systemic potassium homeostasis, as they eliminate more than 90% of a highly variable dietary potassium intake. A number of hormones are involved in maintaining plasma potassium levels within the normal range. Moreover, it was reported that dietary potassium deficiency raises blood pressure and enhances salt sensitivity (8).

The inwardly rectifying K^+ channels (K_{ir}), specifically $K_{ir}4.1$ and $K_{ir}5.1$ K^+ channels (encoded by *Kcnj10* and *Kcnj16* genes, respectively) are thought to play major roles in controlling basolateral membrane potential and potassium recycling in the distal nephron, which is necessary to sustain the Na^+/K^+-ATPase activ-

Conflict of interest: The authors have declared that no conflict of interest exists.

Submitted: December 15, 2016
Accepted: August 8, 2017
Published: September 21, 2017

Reference information:
JCI Insight. 2017;2(18):e92331.
https://doi.org/10.1172/jci.insight.92331.

ity and generate the driving force for Cl^- and Na^+ transport (9, 10). Recent studies suggest that $K_{ir}4.1$ (likely forming heteromeric channels with $K_{ir}5.1$) is essential for modulating Na^+-Cl^- cotransporter (NCC) activity, mediating potassium sensing by distal convoluted tubule (DCT) cells and coupling this signal to apical transport processes (11). *Kcnj10* and *Kcnj16* are highly expressed in the DCT, connecting tubule, and cortical collecting duct (CCD) — nephron segments that are established as major targets for multiple hormones controlling blood pressure. $K_{ir}4.1$ forms either a homotetrameric channel or coassembles with $K_{ir}5.1$ to yield the $K_{ir}4.1/K_{ir}5.1$ heterotetrameric channel (12–14). The heteromeric $K_{ir}4.1/K_{ir}5.1$ channel has unique properties, including single-channel conductance that is greater than that of the homomeric $K_{ir}4.1$ (13–15). We and others reported that the $K_{ir}4.1/K_{ir}5.1$ heteromer is the predominant basolateral K^+ channel in both the DCT and CCD (16–19). In humans, loss-of-function mutations in the *KCNJ10* gene have been shown to cause epilepsy, ataxia, sensorineural deafness and tubulopathy (EAST/SeSAME) syndrome (20–22). The renal phenotype of these mutations includes salt wasting, hypomagnesemia, metabolic alkalosis, and hypokalemia. Experiments with the *Kcnj10*-knockout (*Kcnj10*$^{-/-}$) mice revealed that the lack of $K_{ir}4.1$ resulted in an early postnatal mortality, decreased expression of the NCC (23), and increased levels of β and γ subunits of the epithelial sodium channel (ENaC) (24). Targeted disruption of the *Kcnj16* gene in mice caused hypokalemic, hyperchloremic metabolic acidosis with hypercalciuria (25). Mutations in *Kcnj16* gene are also associated with nonfamilial Brugada syndrome that causes arrhythmias including sudden cardiac death (26); in addition, genome-wide association studies of metabolite quantitative traits identified *Kcnj16* as a candidate gene (27). Furthermore, it was proposed that loss of activation of *Kcnj16* by transcriptional factor HNF1β might result in the development of autosomal dominant tubulointerstitial kidney disease (28). Despite these important findings, the mechanistic role of $K_{ir}4.1/K_{ir}5.1$ (*Kcnj10*/*Kcnj16*) basolateral K^+ channels in the development of salt-sensitive (SS) hypertension and control of electrolyte balance is largely unknown.

Dahl SS rats develop severe hypertension when placed on a high-salt diet and, therefore, represent a well-established research model of SS hypertension (1, 29–31). Remarkably, no studies have aimed to determine the role of $K_{ir}4.1/K_{ir}5.1$ channels in a model of hypertension, nor have any studies evaluated the role of these channels in electrolyte homeostasis when animals were maintained on various diets. Therefore, we created a rat model in which a zinc finger nuclease (ZFN)–induced mutation in *Kcnj16* led to $K_{ir}5.1$ channel knockout in SS rats ($SS^{Kcnj16-/-}$), which enables us to assess the role of the $K_{ir}5.1$ channel and the $K_{ir}4.1/K_{ir}5.1$ heteromer in the development of SS hypertension and control of kidney function. Here, we show that $K_{ir}4.1/K_{ir}5.1$–mediated K^+ transport in the distal nephron contributes meaningfully to SS hypertension. Collectively, these studies provide evidence that $K_{ir}4.1/K_{ir}5.1$ channels are necessary for proper renal electrolyte homeostasis and suggest that their activity is tightly regulated during the development of SS hypertension. Furthermore, we demonstrated that *Kcnj16* is essential for the beneficial effects of a high-potassium diet. Targeting these channels may be attractive for treatment of hyperkalemia, sodium retention, hypertension, as well as some other renal diseases.

Results

ZFN–based null mutation of Kcnj16 in the SS rat. The Dahl SS rat has been a highly useful animal model to study the mechanisms of SS hypertension, as it recapitulates the many phenotypic features found in hypertensive African Americans (1, 31). Changing the dietary sodium content from 0.4% NaCl (low salt; could be also considered as normal) to 4% NaCl (high salt) results in a profound elevation of blood pressure within 2–3 weeks, which is accompanied by a decrease in renal function. Immunohistochemical (IHC) staining showed $K_{ir}5.1$ expression in both the DCT and CCD, where CCDs were identified by the presence of intercalated and principal cells ($K_{ir}5.1$ is expressed in the principal cells only; see ref. 17). We found that in both segments $K_{ir}5.1$ channel expression was significantly elevated in SS rats fed a high-salt diet (4%; 3 weeks) compared with those fed a low (0.4%) salt diet (Figure 1A and Supplemental Figure 1; supplemental material available online with this article; https://doi.org/10.1172/jci.insight.92331DS1). To examine the role of $K_{ir}5.1$ in the development of SS hypertension, we created a *Kcnj16* knockout on a Dahl SS rat background ($SS^{Kcnj16-/-}$) using the ZFN–based gene editing approach (32). A resulting 18-bp deletion (validated by DNA sequencing) led to a 6-amino-acid deletion within the second transmembrane domain (TM2) of the $K_{ir}5.1$ channel (Figure 1B). Despite the predicted in-frame nature of the mutation, a complete absence of $K_{ir}5.1$ expression in $SS^{Kcnj16-/-}$ rats was demonstrated with IHC and Western blotting. As shown in Figure 1D, $K_{ir}5.1$ is highly expressed at the basolateral membranes of the CCDs and DCTs (localization

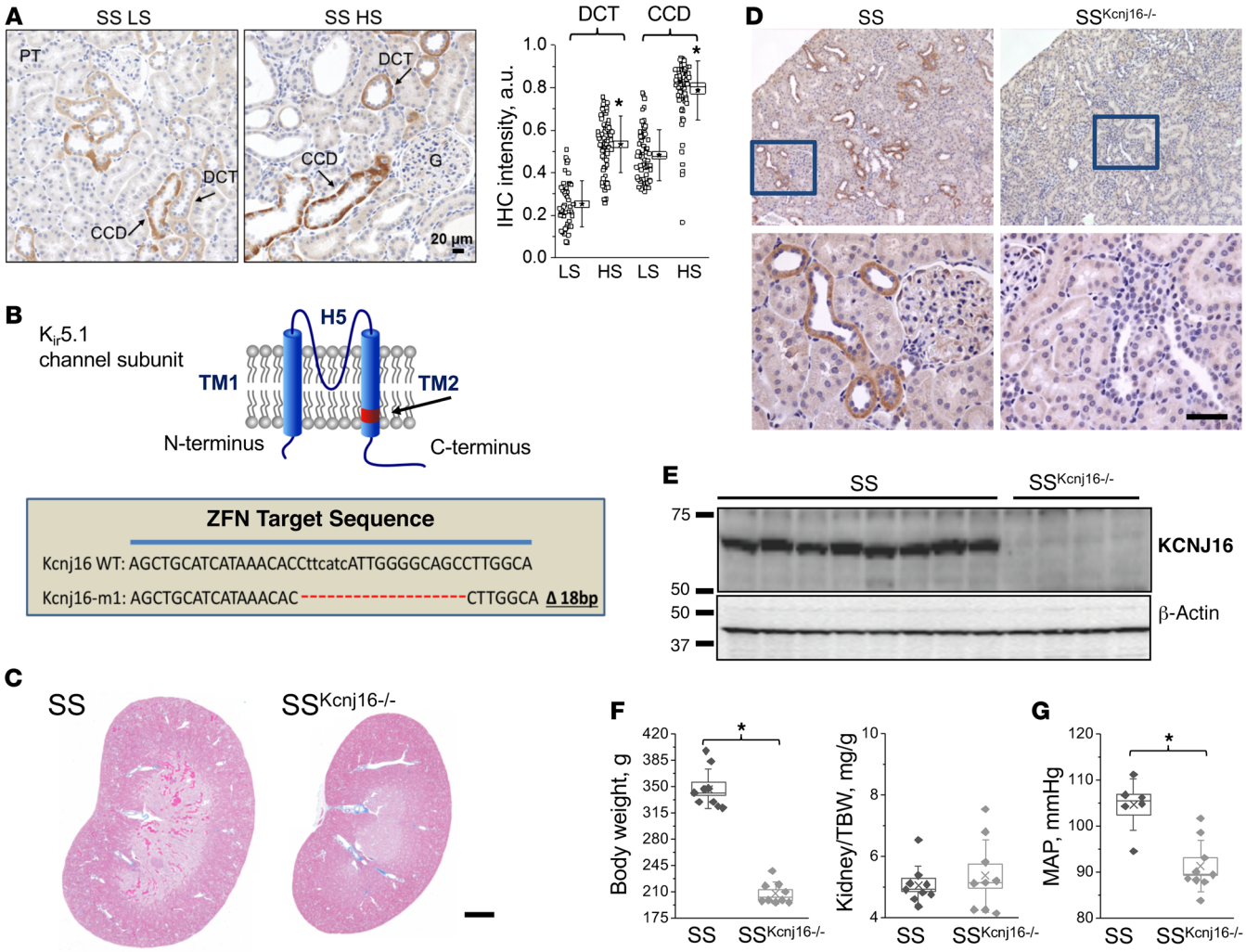

Figure 1. Kcnj16 knockout in the Dahl SS rat. (**A**) Immunostaining for Kcnj16 (K$_{ir}$5.1) basolateral channels in salt-sensitive (SS) rats fed low salt (LS; 0.4% NaCl) or high salt (HS; 4% NaCl, 3 weeks). Note absence of protein staining in collecting duct (CD) intercalated cells. Right panel shows summary graphs of K$_{ir}$5.1 expression in distal convoluted tubule (DCT) and cortical CD (CCD) on LS and HS diets. *N* = 5 rats; *n* ≥ 46 tubules for each group. (**B**) A scheme of *Kcnj16* gene showing the location of zinc finger nuclease–caused (ZFN-caused) deletion. Also shown is a specific position of deletion in the second transmembrane domain (TM2) of the protein. (**C**) A representative section of Masson's trichrome–stained kidney from 12-week-old SS and SS$^{Kcnj16-/-}$ rats fed a LS diet. Scale bar: 2 mm. (**D**) An immunohistochemical analysis of the rat kidney tissues shows complete absence of *Kcnj16* protein in SS$^{Kcnj16-/-}$ rats (right) compared with SS rats (left). Top and bottom images are at ×10 and ×40 magnification, respectively. Scale bar: 50 μm. (**E**) Western blotting analysis of K$_{ir}$5.1 expression in the kidney cortex of SS and SS$^{Kcnj16-/-}$ rats. Each line represents 1 rat. (**F**) Body weight of age-matched SS and SS$^{Kcnj16-/-}$ rats fed a 0.4% NaCl diet. Normalized kidney per total body weight (TBW) is also shown (*N* = 15). (**G**) Mean arterial pressure (MAP) in SS and SS$^{Kcnj16-/-}$ rats when animals were fed a 0.4% NaCl diet (*N* ≥ 9 rats in each group) measured with telemetry. Comparisons between groups were made using 1-way ANOVA. *$P < 0.05$.

at specific nephron segments was confirmed with double staining with antibodies targeting aquaporin-2 (Aqp2) and the NCC, markers of collecting duct principal cells and DCTs, respectively; data not shown). No K$_{ir}$5.1 immunoreactivity was observed in the kidney sections from the SS$^{Kcnj16-/-}$ rats, which is consistent with Western blotting analysis (Figure 1E).

Role of K$_{ir}$5.1 in the control of blood pressure and kidney function. The *Kcnj16* knockout in the SS rat resulted in changes in growth and development (reduction in body weight; Figure 1F). SS$^{Kcnj16-/-}$ rats also had smaller kidneys (Figure 1C; normalized kidney per total body weight [TBW] was not different between strains — Figure 1F), and exhibited lower mean arterial pressure (MAP) compared with SS rats when they were fed a low-salt (0.4% NaCl) diet (Figure 1G).

Analyses of microalbuminuria, protein casts, glomerular damage, plasma aldosterone, blood urea nitrogen (BUN), and glomerular filtration rate (GFR) were performed in SS$^{Kcnj16-/-}$ and control SS rats fed a 0.4% salt diet to assess potential changes in kidney function and renal injury. The renal histological changes represented by the percentage of protein casts and glomerular injury score (Figure 2, A and B)

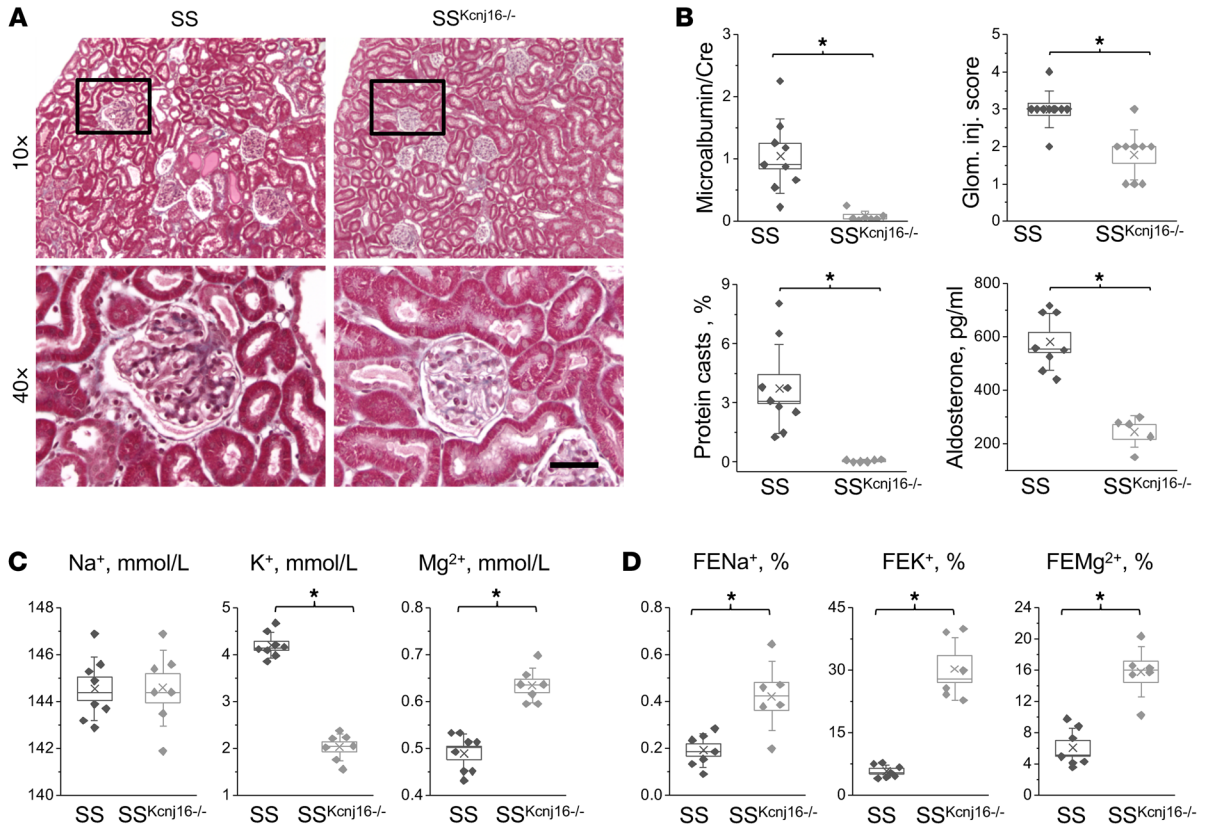

Figure 2. Kidney function and electrolyte balance in SS$^{Kcnj16-/-}$ rats. (**A**) Light microscopy of Masson's trichrome–stained sections of kidney cortex (at ×10 and ×40 magnification) of salt-sensitive (SS) and SS$^{Kcnj16-/-}$ rats fed a 0.4% NaCl diet. Scale bar: 50 μm. (**B**) Renal injury as assessed by measuring albumin (normalized to creatinine) in urine samples collected for 24 hours in SS and SS$^{Kcnj16-/-}$ rats ($N \geq 7$). The averaged percentage of protein casts, glomerular injury, and the plasma aldosterone concentrations in SS and SS$^{Kcnj16-/-}$ rats are also shown ($N \geq 6$ rats). For glomeruli scoring, each point is an average of 80 glomeruli per rat. (**C**) Biochemical analyses of electrolytes in plasma samples collected from SS and SS$^{Kcnj16-/-}$ rats (8–9 weeks old; 0.4% NaCl diet; $N = 10$). (**D**) Fractional excretion (FE) of Na^+, K^+, and Mg^{2+} over a 24-hour period in SS and SS$^{Kcnj16-/-}$ rats ($N = 7$). Comparisons between groups were made using 1-way ANOVA. *$P < 0.05$.

were both significantly improved in SS$^{Kcnj16-/-}$ rats. Consistent with this, the albumin excretion (normalized to creatinine) was significantly lower in SS$^{Kcnj16-/-}$ rats. Plasma aldosterone concentration was found to be significantly lower in SS$^{Kcnj16-/-}$ rats (Figure 2B). We also observed a decrease in GFR that likely reflects the physiological response to a decreased blood pressure (Supplemental Figure 2A) and an increase in plasma BUN (Supplemental Figure 2B) in SS$^{Kcnj16-/-}$ rats.

Biochemical analyses of plasma samples revealed that SS$^{Kcnj16-/-}$ rats develop severe hypokalemia and hypermagnesemia, but no changes in blood Na^+ level (Figure 2C). Fractional excretion analyses demonstrated that SS$^{Kcnj16-/-}$ rats have a salt-wasting phenotype with increased fractional excretion of Na^+, K^+, and Mg^{2+}, respectively (Figure 2D).

$K_{ir}4.1$ and $K_{ir}5.1$ are the main K^+ channels in the basolateral membrane of DCTs and CCDs responsible for K^+ recycling in these segments (9, 16, 17). Figure 3A illustrates that $K_{ir}5.1$ is expressed on the basolateral membrane of both DCTs and CCDs (see also Supplemental Figure 3). We further employed a single-channel analysis of patch-clamp approach to investigate the functional properties of the basolateral K^+ conductance in isolated CCDs of SS and SS$^{Kcnj16-/-}$ rats. Electrophysiological recordings of basolateral K^+ channels in the CCDs from SS$^{Kcnj16-/-}$ rats (Figure 3B shows a representative tubule used for patch-clamp studies) revealed activity of only homomeric $K_{ir}4.1$ channels. Control SS rats had both 48- and 25-pS channels, indicating heteromeric $K_{ir}4.1/K_{ir}5.1$ and homomeric $K_{ir}4.1$ channels, respectively (Figure 3, C and D). Calculated channel open probability (P_o) was 0.55 ± 0.10 and 0.55 ± 0.07 at –60 and –80 mV holding potentials and 0.78 ± 0.05 and 0.84 ± 0.05 at the same voltage for heteromeric and homomeric channels, respectively. In contrast, SS$^{Kcnj16-/-}$ rats revealed activity of only small homomeric $K_{ir}4.1$ channels (P_o was 0.66 ± 0.04 and 0.61 ± 0.07 at –60 and –80 mV holding potentials) (Figure 3, E and F). No voltage P_o dependence was observed.

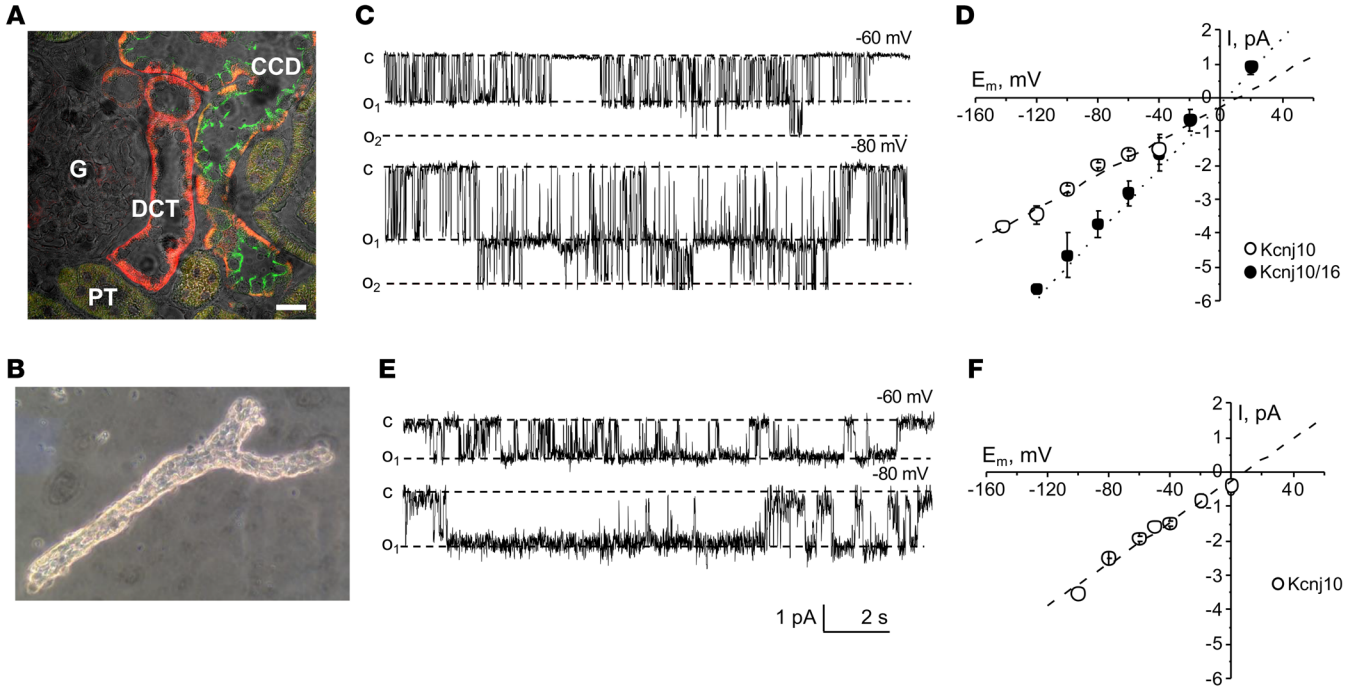

Figure 3. Electrophysiological analysis of $K_{ir}4.1$ homotetrameric and $K_{ir}4.1/K_{ir}5.1$ heterotetrameric channels in SS and $SS^{Kcnj16-/-}$ rats. (**A**) Double-immunostaining images show Kcnj16 expression (red) in the distal convoluted tubule (DCT) and cortical collecting duct (CCD) cells. Aqp2 (green) was used as a marker of CD principal cells. Proximal tubules (PTs) and glomerulus (G) are also shown. Scale bar: 20 μm. (**B**) Representative manually isolated distal tubule (note bifurcation) used for the patch-clamp analysis on basolateral membrane. (**C** and **D**) Representative current traces (**C**) and average current-voltage (I/V) relationships (**D**) of the unitary current amplitude of 25.4 ± 3.9 pS ($K_{ir}4.1$) and 48.1 ± 0.2 pS ($K_{ir}4.1/K_{ir}5.1$) K^+ channels measured in salt-sensitive (SS) rats. (**E** and **F**) Representative current traces and average I/V relationships assessed in $SS^{Kcnj16-/-}$ rats ($N \geq 5$).

We also assessed if there were compensatory changes in $K_{ir}4.1$ (*Kcnj10*) expression in the absence of *Kcnj16* in the $SS^{Kcnj16-/-}$ rats. As shown in Figure 4A and summarized in Figure 4B, Kcnj10 expression was significantly increased in $SS^{Kcnj16-/-}$ rats. However, an IHC analysis revealed that Kcnj10 channels were predominantly expressed in the cytosol in $SS^{Kcnj16-/-}$ rats in contrast to strong basolateral localization of this channel in SS rats (Figure 4, C and D). These data suggest that $K_{ir}5.1$ is required for proper trafficking and localization of both $K_{ir}4.1$ homomeric and $K_{ir}4.1/K_{ir}5.1$ heteromeric channels to the basolateral membrane of both DCT and CCD segments.

Effects of a Kcnj16 knockout on sodium reabsorption in the DCT and TAL. First, expression of NCC was analyzed to assess changes in transporters mediating sodium absorption in DCTs. Since it was reported that *Kcnj10* is expressed in the cortical part of the thick ascending limb of Henle's loop (TAL) (20, 33), we also explored the abundance of the Na^+-K^+-Cl^- cotransporter (NKCC2), the main Na^+ transporter in TAL. Both the total and phosphorylated (active) forms of NKCC2 and NCC were analyzed. We detected an upregulation of total NCC as well as active p-NCC levels in $SS^{Kcnj16-/-}$ rats compared with SS rats (Figure 5, A and C). Similarly, total and phosphorylated NKCC2 were elevated in $SS^{Kcnj16-/-}$ rats (Figure 5, B and D).

Physiological consequences of a Kcnj16 knockout upon salt-induced hypertension and renal injury. To test the effect of a high-salt diet and define the role of Kcnj16 in the development of SS hypertension, we performed the analysis of various physiological parameters of $SS^{Kcnj16-/-}$ rats when they were switched from a low-salt (0.4%) to high-salt (4%) diets. Remarkably, none of the studied $SS^{Kcnj16-/-}$ rats survived more than 4 days after the diet change, and approximately half of the animals died within the first 24 hours of beginning the high-salt diet. The survival rates of SS and $SS^{Kcnj16-/-}$ rats (both male and female) fed a 4% salt diet are shown in Figure 6A. Urine and blood were collected and analyzed in SS and $SS^{Kcnj16-/-}$ rats 1 day before and 1 day after switching to a high-salt diet in those rats able to survive more than 24 hours when fed the high-salt diet. Figure 6B summarizes Na^+ and K^+ concentrations in urine (normalized to creatinine) and plasma in $SS^{Kcnj16-/-}$ rats before and 24 hours after a high-salt diet. As presented in this figure, high salt intake rapidly increases the excretion of both Na^+ and K^+, and significantly lowers the blood electrolyte concentrations. Thus, blood K^+ was reduced to less than 1.4 mmol/l. This severe hypokalemia is likely the

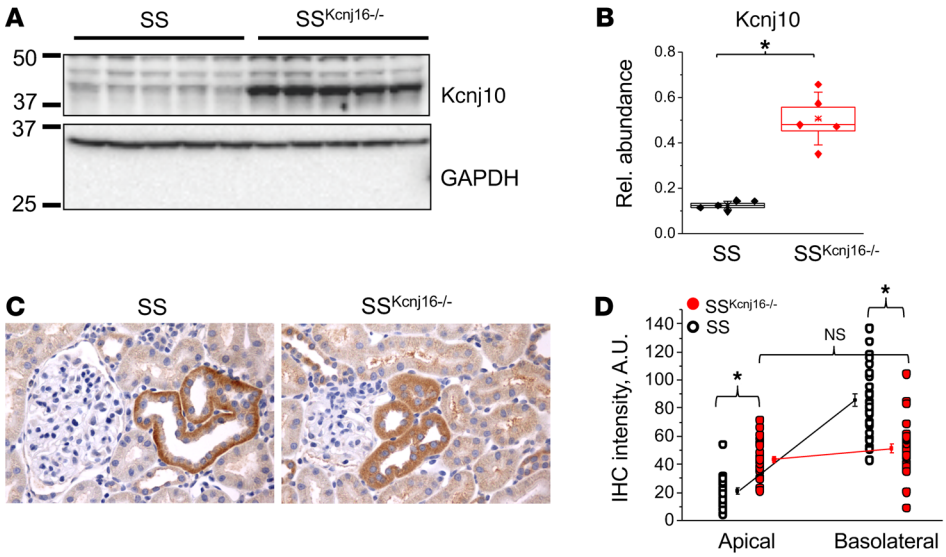

Figure 4. Expression and localization of Kcnj10 in SS and SS$^{Kcnj16-/-}$ rats. (**A** and **B**) Western blotting analysis of renal cortex tissues from salt-sensitive (SS) and SS$^{Kcnj16-/-}$ rats. The blot was probed with Kcnj10 antibodies. Equal loading was verified by blotting with GAPDH. (**C**) Representative IHC staining of kidney cortical sections for detection of Kcnj10 protein in SS and SS$^{Kcnj16-/-}$ rats at magnification ×40. (**D**) Summary graph of the analysis of Kcnj10 protein distribution on apical/basolateral sides in the distal tubules of SS and SS$^{Kcnj16-/-}$ rats ($N \geq 5$ rats, $n = 58$ tubules for each group). Comparisons between groups were made using 1-way ANOVA. *$P < 0.05$. NS, not significant

cause of death in SS$^{Kcnj16-/-}$ rats, as it is known to result in respiratory paralysis and/or fatal arrhythmia and sudden cardiac arrest (34).

We further tested the effects of inhibitors of sodium channels and transporters critical for the maintenance of electrolyte homeostasis in the TALs, DCTs, and collecting ducts. The ENaC inhibitor benzamil (15 mg/l in drinking water) was able to rescue SS$^{Kcnj16-/-}$ rats from mortality induced by a high-salt diet. Removal of benzamil from drinking water resulted in SS$^{Kcnj16-/-}$ rat mortality. In contrast, supplementation of drinking water with hydrochlorothiazide (HCTZ; 75 mg/l) only slightly delayed the animals' death. Interestingly, the effect of HCTZ was more profound in male compared with female subjects. Furosemide (15 mg/l) did not have any effects (Figure 6C); it was also tested at a higher concentration (150 mg/l) with the same outcome. Neither male nor female rats survived more than 3 days ($N = 3$ for each gender) when supplemented with furosemide.

High-potassium diet plays a protective role in Kcnj10/16–mediated abnormalities. Knockout of *Kcnj16* in SS rats induces a severe renal phenotype that, apart from hypokalemia, is characterized with a lower blood pressure, decreased body/kidney weight, and 100% mortality within a few days when fed a high-salt diet. It was previously reported that dietary potassium deficiency, common in modern diets, raises blood pressure and enhances salt sensitivity (2, 8, 35). Thus, we next supplemented the high-NaCl diet with high K^+ in an attempt to counteract the likely fatal hypokalemia observed in SS$^{Kcnj16-/-}$ rats on high-Na^+ diet and determine the relative contribution of $K_{ir}4.1/K_{ir}5.1$ channels in the protective effect of high-K^+ diet in salt-induced hypertension. Three groups of animals were fed a high-NaCl diet (4%) for 5 weeks; 1 group of SS rats was not supplemented with high potassium (0.36% KCl) and 2 other groups (both SS and SS$^{Kcnj16-/-}$) were fed a diet supplemented with additional 2% KCl (total was 2.36% KCl). As shown in Figure 7A, after 5 weeks on a high-salt diet, MAP was reduced in SS rats supplemented with high potassium (compared with control SS rats). Importantly, our experiments revealed that all SS$^{Kcnj16-/-}$ rats survived when fed a high-salt diet supplemented with high potassium (see Figure 6A for comparison). Furthermore, blood pressure did not change in SS$^{Kcnj16-/-}$ fed a high-K^+ diet, which together with the observation that Kcnj16 expression increases in SS rats fed a high-salt diet demonstrates a critical role of this channel in the development of salt-induced hypertension. Consistent with this conclusion, the development of albuminuria, the hallmark of SS hypertension and kidney damage in SS rats, was significantly lower in SS$^{Kcnj16-/-}$ rats for all experimental data points (Figure 7B).

Circadian variations of MAP before and 5 weeks after a high-salt diet are shown in Supplemental

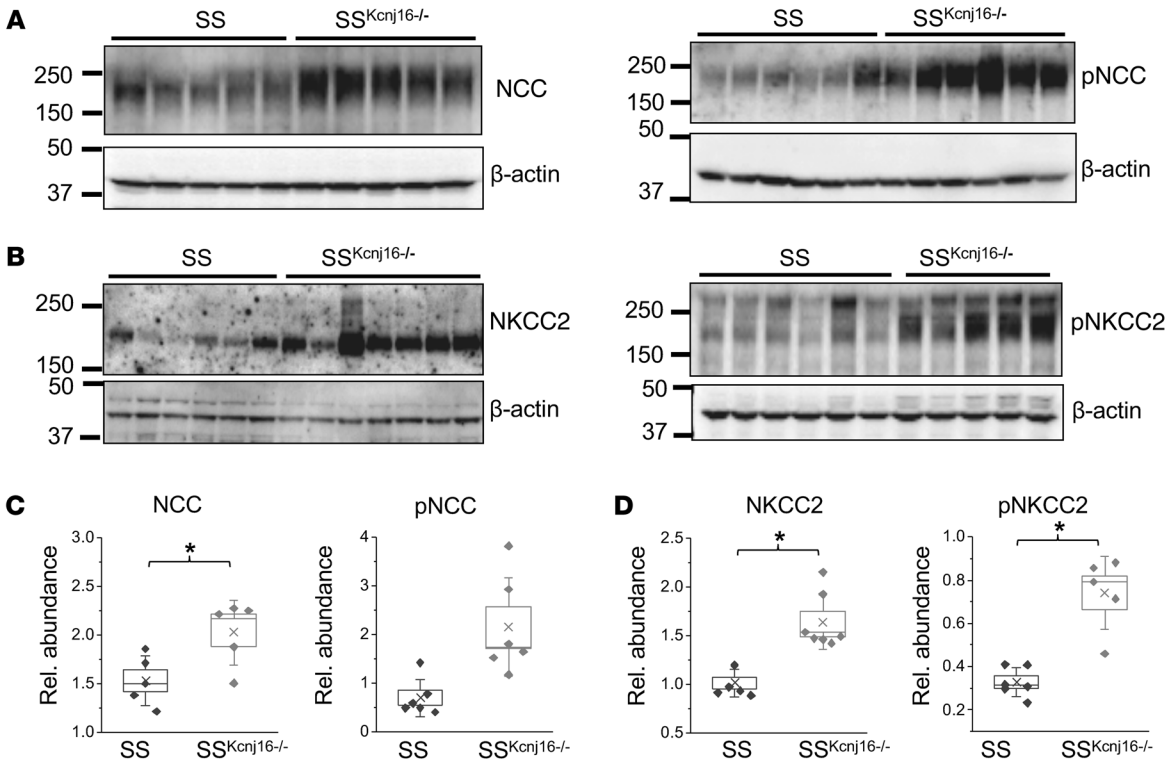

Figure 5. Differences in NCC and NKCC2 expression in SS$^{Kcnj16-/-}$ rats. Western blotting analysis of NCC (**A**) and NKCC2 (**B**) from the kidney cortex lysates of salt-sensitive (SS) and SS$^{Kcnj16-/-}$ rats. Active phosphorylated forms were also analyzed. Each line represents 1 rat. (**C** and **D**) Summary graphs showing the average relative density of the bands (normalized to loading controls) in the studied groups. *$P < 0.05$ versus SS rats. Comparisons between groups were made using 1-way ANOVA.

Figure 4A. The heart rate was lower in SS$^{Kcnj16-/-}$ rats compared with SS rats when fed a normal-salt diet, whereas a high-salt diet decreased heart rates in all groups (Supplemental Figure 4B). Shown in Figure 7C are summary graphs of the main electrolyte concentrations in urine normalized to creatinine, which demonstrate electrolyte balance in all studied groups (see also Supplemental Figure 5 for a summary of electrolyte homeostasis during the development of salt-induced hypertension). Importantly, as seen in Figure 7C, electrolyte/creatinine ratios were similar between SS and SS$^{Kcnj16-/-}$ rats when animals were fed a 0.4% NaCl diet, which allows us to assume that food intake was similar in the studied groups. Hematocrit levels also did not differ in SS and SS$^{Kcnj16-/-}$ rats fed a 0.4% NaCl diet (46.00% ± 1.45% and 44.81% ± 0.57% in SS and SS$^{Kcnj16-/-}$ rats, respectively; $N = 5$ and 6 rats, $P = 0.631$).

To further delineate the contribution of high-K^+ diet and the Kir5.1 channel to the regulation of sodium absorption during the development of salt-induced hypertension in SS rats, we measured the expression of NKCC, p-NKCC, NCC, p-NCC, and all 3 ENaC subunits (including truncated forms of α- and γ-ENaC subunits) in homogenates from the kidney cortex lysates of SS rats fed either a high-salt diet (4% NaCl) or a 4% NaCl diet supplemented with high K^+ and SS$^{Kcnj16-/-}$ rats fed a 4% NaCl diet supplemented with high K^+. As shown in Figure 8, A and B, and summarized in Figure 8C, expression of both total NKCC2 and NCC was increased in SS$^{Kcnj16-/-}$ rats fed a 4% diet supplemented with high K^+ compared with SS fed a high-salt diet either supplemented or not with high K^+. NKCC2 expression was reduced when SS rats were fed a 4% salt diet supplemented with high K^+. Levels of p-NKCC or p-NCC were not significantly different between groups. Expression of α- and β-ENaC subunits was increased when SS rats were fed a high-salt diet supplemented with high K^+. Interestingly, expression of α-ENaC was increased in SS$^{Kcnj16-/-}$ rats fed a 4% diet supplemented with high K^+ compared with SS fed a high-salt diet with high K^+, but expression of β-ENaC and cleaved γ-ENaC was decreased compared with the same group. When considering these data, it should be taken into account that SS rats were fed a high-salt diet for 5 weeks and, as it was previously shown, expression of sodium transporters is inappropriately regulated in SS rats compared with salt-resistant animals. For instance, ENaC expression (and activity) is upregulated in SS rats when animals are fed a

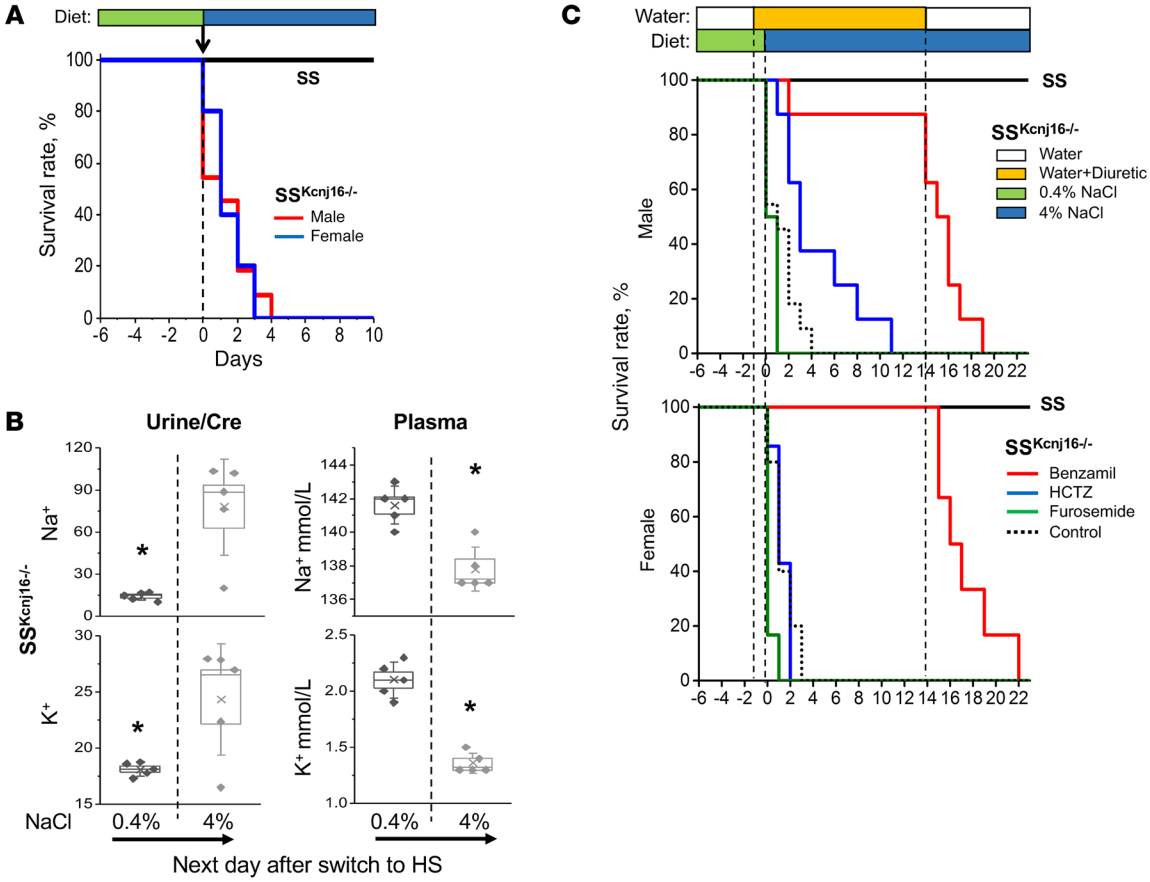

Figure 6. High salt intake triggers rapid mortality of SS$^{Kcnj16-/-}$ rats. (**A**) Survival rate of salt-sensitive (SS) and SS$^{Kcnj16-/-}$ rats on a 4% NaCl diet (N = 20 and 5 for male and female rats, respectively). (**B**) Na^+ and K^+ concentrations in urine (normalized to creatinine) and plasma in SS$^{Kcnj16-/-}$ rats before and 24 hours after the diet switch from 0.4% to 4% NaCl ($N \geq 5$ rats for each group). Comparisons between groups were made using 1-way ANOVA. *$P < 0.05$. HS, high salt. (**C**) Survival rate of SS$^{Kcnj16-/-}$ rats when a high-salt diet was supplemented with water containing diuretics. Benzamil and furosemide were added to drinking water at a concentration of 15 mg/l, and hydrochlorothiazide (HCTZ) at 75 mg/l. N = 7/6, 8/6, and 8/7 (male/female rats) for experiments with benzamil, furosemide, and HCTZ, respectively.

high-salt diet (36–38), whereas in salt-resistant animals, high salt results in inhibition of ENaC (39).

Dietary potassium loading results in rapid kaliuresis, diuresis, and natriuresis (7, 40, 41), and the next aim was to test the effect of high-K^+ supplementation in SS$^{Kcnj16-/-}$ rats on body and kidney weights. As summarized in Figure 9, the kidney and body weights of SS$^{Kcnj16-/-}$ rats were significantly improved when the dietary potassium content was increased. Figure 10 summarizes our hypothesis regarding the role of $K_{ir}4.1/K_{ir}5.1$ channels in the kidney function and blood pressure control based on the SS$^{Kcnj16-/-}$ model.

Discussion

In the kidney, discretionary Na^+ reabsorption and K^+ secretion in the aldosterone-sensitive distal nephron is a determinant of the pressure-natriuresis relationship, which is of fundamental importance in the long-term control of arterial pressure (42–44). Importantly, dietary potassium deficiency raises blood pressure and enhances salt sensitivity by changing cell membrane voltage (resulting in hyperpolarization) and stimulating NCC activation (8). Specific K_{ir} channels, including $K_{ir}4.1$ and $K_{ir}5.1$, play a dominant role in determining resting membrane potential and spatial K^+ buffering. One of the primary functions of basolateral $K_{ir}4.1/K_{ir}5.1$ channels is to recycle K^+ across the basolateral membrane for proper function of the Na^+-K^+. Mutations of these channels in humans can cause severe disease phenotypes (20–22, 26), but their role in the development of SS hypertension was never investigated. The strain of the re-derived Dahl SS rat used in our studies (SS/JrHsdMcwi) has been inbred for more than 50 generations and is a practically proven model for the study of SS hypertension (31, 45, 46).

$K_{ir}5.1$ typically does not form a functional homomeric K^+-conducting channel in the absence of another

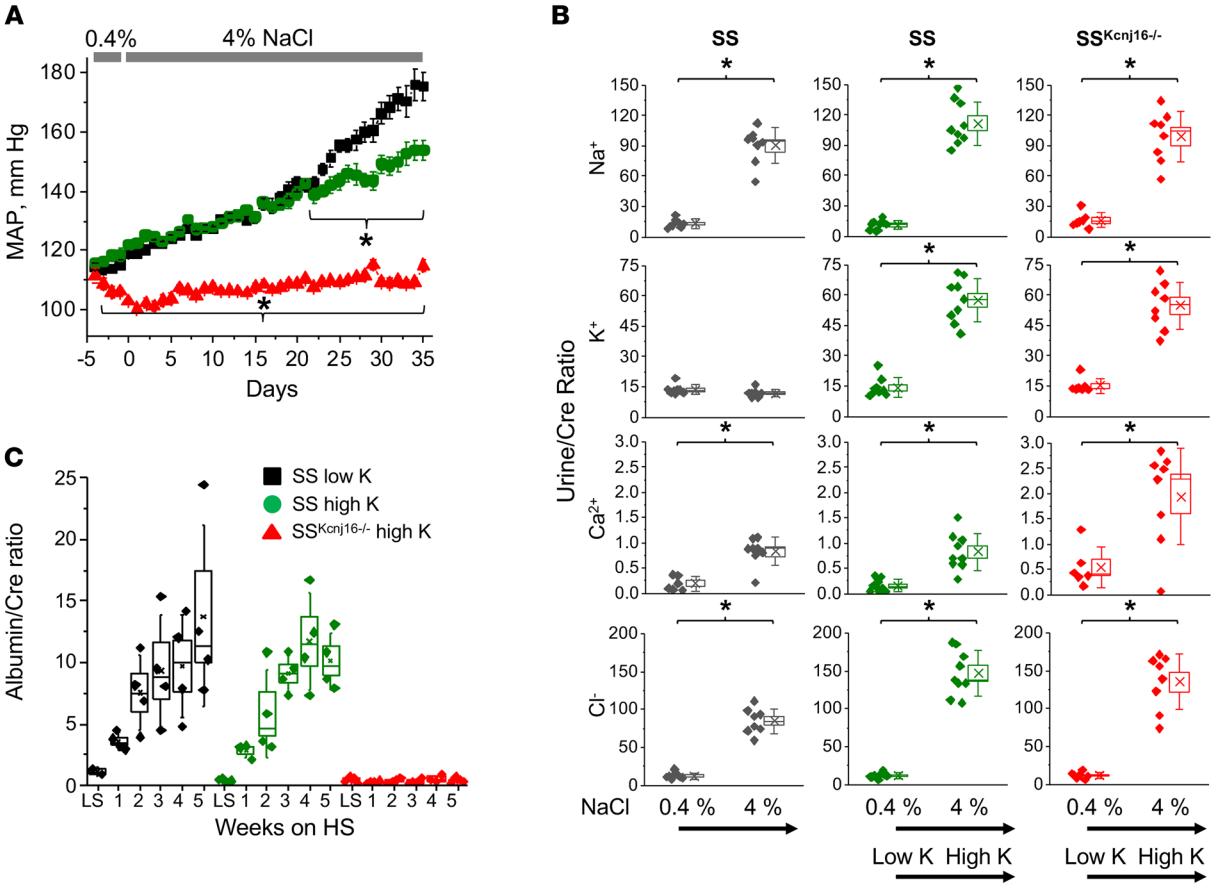

Figure 7. The combination of a high-potassium diet and $K_{ir}5.1$ channel deletion mediate the protective effects on the development of SS hypertension. (**A**) Mean arterial pressure (MAP) in salt-sensitive (SS) and $SS^{Kcnj16-/-}$ rats. Blood pressure was measured with radiotelemetry (see also Supplemental Figure 3 for circadian rhythms and heart rate analyses). Animals were switched from a 0.4% to a 4% NaCl diet at day 0. Then, SS rats were fed either a standard 4% NaCl diet (black, $N = 10$ rats) or a 4% NaCl diet supplemented with high K^+ (2% KCl; red, $N = 14$). $SS^{Kcnj16-/-}$ rats were fed a 4% NaCl diet supplemented with high K^+ (green, $N = 8$). Comparisons between groups were made using repeated-measures ANOVA. * $P < 0.05$ versus SS rats fed a low-K^+ diet. (**B**) Development of albuminuria (albumin to creatinine ratio) in the same groups of animals ($N \geq 8$ rats). (**C**) Urinary electrolyte analysis of rats used in the experimental protocol shown in **A**; bars indicate electrolyte concentrations in control (0.4% NaCl [LS] or before diet change) and at the end of the experiment (4% NaCl [HS] and with or without K^+ supplement) for all groups of animals ($N = 8$–13 rats in each group; see also Supplemental Figure 4). Comparisons between groups were made using 1-way ANOVA. * $P < 0.05$ versus SS rats fed a 0.4% NaCl diet.

related subunit, and the resulting $K_{ir}4.1/K_{ir}5.1$ heteromeric channel is clearly distinguishable from the $K_{ir}4.1$ homomeric channel (9, 15). It was previously thought that $K_{ir}4.1$ was the dominant channel driving basolateral K^+ recycling in the distal tubule, whereas $K_{ir}5.1$ was considered to have a modulatory role by increasing conductance and blunting pH sensitivity (10). Indeed, loss-of-function mutations in *Kcnj10* cause SeSAME/EAST syndrome associated with hypotension and a severe salt wasting tubulopathy in humans and animal models (20–22). In contrast, *Kcnj16* deletion in mice does not lead to urinary salt wasting and reduced blood pressure due to the compensation by *Kcnj10* (25). However, as we report here, *Kcnj16* knockout in a rat model of SS hypertension dramatically alters these conclusions. These $SS^{Kcnj16-/-}$ rats exhibit a renal phenotype reminiscent of SeSAME/EAST and *Kcnj10* deletion: salt wasting, hypomagnesemia, and hypokalemia. Interestingly, we detect prominent retention of $K_{ir}4.1$ in the cytosol with only a small number of channels present on the basolateral membrane, suggesting interdependence of proper translocation of both channels in the setting of SS hypertension. This is the opposite of the marked upregulation of plasma membrane $K_{ir}4.1$ in normotensive mice lacking *Kcnj16* (25). It needs to be further determined whether this feature is common for hypertensive or conditionally hypertensive animal models.

We demonstrate here that the salt-wasting phenotype of $SS^{Kcnj16-/-}$ rats occurs despite compensatory increased total and phosphorylated levels of the major Na^+ transporters in the TAL and DCT: NKCC2 and NCC, respectively. We hypothesize that the augmented capacity for the apical sodium entry is diminished

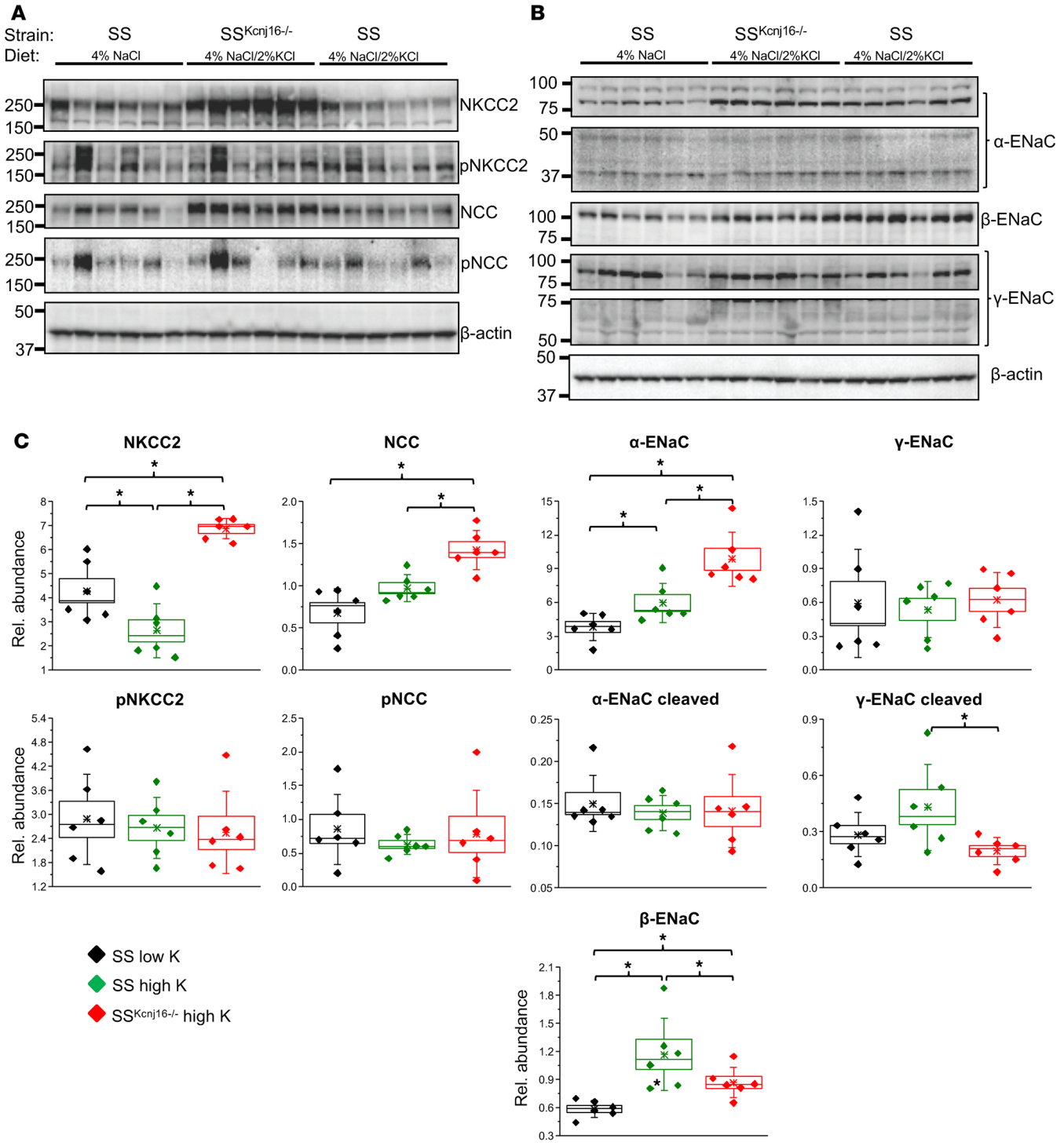

Figure 8. Changes in ENaC, NCC, and NKCC2 expression in SS and SS$^{Kcnj16-/-}$ rats fed a high-potassium diet. Western blotting analysis of NCC, p-NCC, NKCC2, and p-NKCC (**A**) and α-, β-, and γ-ENaC subunits (truncated forms of α- and γ-ENaC subunits are also shown) (**B**) from the kidney cortex lysates of salt-sensitive (SS) rats were fed either a standard 4% NaCl diet or a 4% NaCl diet supplemented with high K^+ (2% KCl) and SS$^{Kcnj16-/-}$ rats fed a 4% NaCl diet supplemented with high K^+. Each line represents 1 rat. (**C**) Summary graphs represent the average relative density of the bands (normalized to loading controls) in the groups. Comparisons between groups were made using 1-way ANOVA. *$P < 0.05$.

by the lack of $K_{ir}4.1/K_{ir}5.1$–mediated basolateral K^+ recycling essential for the Na^+/K^+-ATPase activity. This, in turn, leads to increased fluid delivery to the CD system, where ENaC-mediated sodium entry (in an attempt to conserve sodium) will lead to mandatory apical K^+ secretion in order to sustain activity of the basolateral pump, thereby producing profound kaliuresis and hypokalemia. This state is also exacerbated

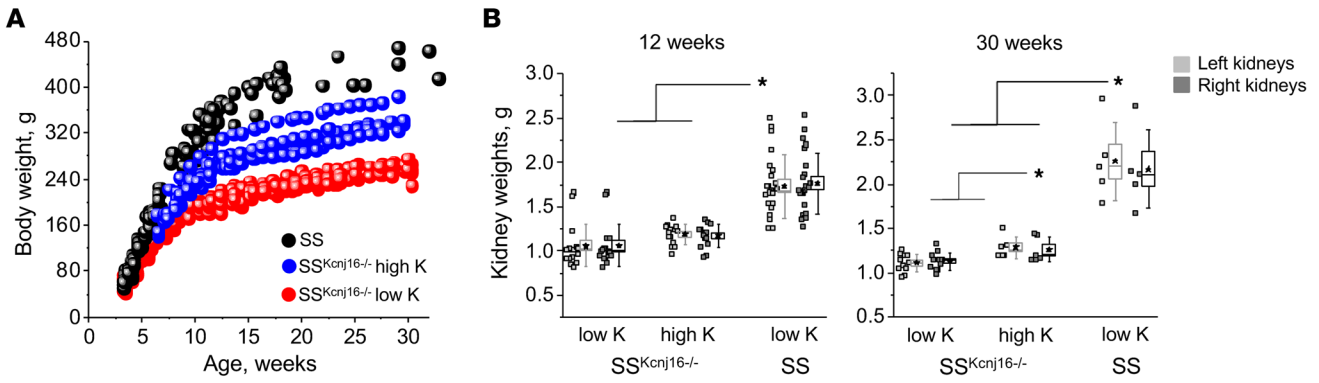

Figure 9. High-potassium diet supplement restores the development of SS$^{Kcnj16-/-}$ rats. (**A**) The effect of a high-potassium diet (2% KCl) on body weight in SS$^{Kcnj16-/-}$ rats. (**B**) Changes in kidney mass of salt-sensitive (SS) and SS$^{Kcnj16-/-}$ rats on low (0.36% K^+) and high (1.41% K^+) potassium–containing diets. Comparisons between groups were made using 1-way ANOVA. *$P < 0.05$.

when SS$^{Kcnj16-/-}$ rats are challenged with a high-salt diet, which is reported to cause a paradoxic upregulation of ENaC activity in SS rats (36). This exacerbates K^+ wasting and drives plasma K^+ to levels incompatible with survival. Importantly, our data with diuretics targeting NKCC, NCC, and ENaC revealed that only potassium-sparing diuretic benzamil, which is an inhibitor of ENaC, rescued SS$^{Kcnj16-/-}$ rats when they were challenged with a high-salt diet. Therefore, the role for ENaC in SS$^{Kcnj16-/-}$ rats seems potentially interesting and requires further investigation.

Dietary potassium supplementation rescued SS$^{Kcnj16-/-}$ rats from mortality induced by a high-salt diet and allowed us to estimate the contribution of $K_{ir}5.1$ channels in the pathology of salt-induced hypertension. The ability of K^+ supplementation to mitigate elevated blood pressure has long been recognized (47). Consistently, the Dietary Approaches to Stop Hypertension (DASH) diet, a diet that is low in sodium and replete with potassium, calcium, and magnesium, is sponsored by the National Heart, Lung, and Blood Institute and now is being recommended as a standard lifestyle modification for patients with hypertension or other cardiovascular risk factors (48, 49). The beneficial effects of dietary potassium are most likely related to the reduced activity of NKCC2 and NCC. It was recently reported that NCC activity in the DCT is induced by augmented plasma K^+ (41, 50). The rapid phosphorylation of NCC in response to a low-potassium diet involves activation of WNK/SPAK by decreased intracellular Cl^- concentrations due to hyperpolarization of the cell membrane in the DCT cells (8, 51). However, recent studies by Penton et al. demonstrated that dephosphorylation of NCC during high-K^+ diet is mediated through a Cl^--independent pathway, which requires further investigation (52). We have observed in our studies that expression of both NCC and NKCC2 was increased in SS$^{Kcnj16-/-}$ rats compared with SS rats fed a high-salt diet either supplemented with high K^+ or not. Expression of ENaC subunits was also modulated in animals supplemented with high K^+, which together with the observation that benzamil rescues SS$^{Kcnj16-/-}$ rats when animals fed a high-salt diet, also supports the hypothesis that $K_{ir}5.1$ channels are important for its regulation. When considering these data, it should be taken into account that all these studies were performed in a model of SS hypertension. It should be noted that a high-potassium diet attenuated blood pressure in SS rats, even when the animals were challenged with a high-salt diet. In contrast, $K_{ir}5.1$ deletion completely precluded elevations of blood pressure caused by high salt in the SS background. This emphasizes the overarching role of basolateral K^+ recycling, and particularly $K_{ir}5.1$ channels, in orchestrating SS apical Na^+ reabsorption in the distal tubule and collecting ducts.

The broad significance of this study is that, with the identification of the indispensable importance of $K_{ir}5.1$ channels in the development and pathology of SS hypertension, we demonstrate how disruption of this channel alters the balance of both Na^+ and K^+, which cannot be compensated by any other factors, and invariably leads to rapid death when animals are kept on a high-salt diet. These data further suggest that $K_{ir}5.1$ channels are a key component of the protective mechanism of high K^+ in many diets, such as the DASH diet. We propose that targeting $K_{ir}5.1$ function clinically could have multiple beneficial actions, in either preventing or mitigating SS hypertension as well as managing various hyperkalemic states. In summary, these data provide evidence that modulation of K^+ secretion in the kidneys by diet manipulation or by targeting $K_{ir}5.1$ may be a powerful tool for the attenuation of high blood pressure during the development of SS hypertension.

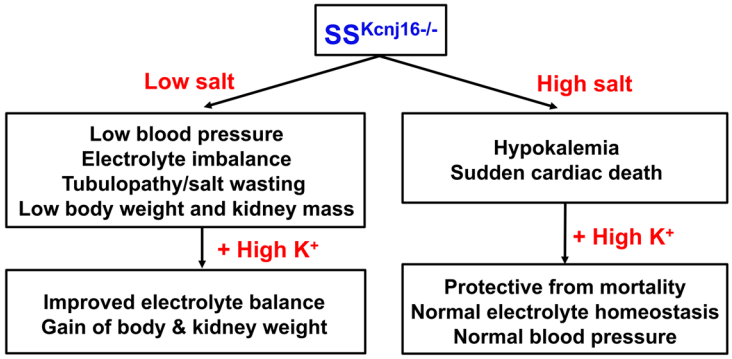

Figure 10. Summary of the proposed role of K_{ir}4.1/5.1 in the kidney function and blood pressure control based on the $SS^{Kcnj16-/-}$ model.

Methods

Animals. Male and female rats were obtained at weaning from colonies developed and maintained at the Medical College of Wisconsin under controlled environmental conditions with parents and offspring fed a purified AIN-76A rodent food (Dyets, Inc.; D113755) containing 0.4% NaCl with water provided ad libitum.

Generation of $SS^{Kcnj16-/-}$ mutant rats. *Kcnj16* gene knockout on the genetic background of the Dahl SS rat was produced using ZFN mutagenesis as described previously (32, 53). Briefly, ZFNs targeting the *Kcnj16* exon 1 sequence AGCTGCATCATAAACACCttcatcATTGGGGCAGCCTTGGCA, where each ZFN binds to each underlined sequence on complementary strands were obtained from Sigma-Aldrich. In vitro–transcribed mRNAs encoding ZFNs were injected into SS/JrHsdMcwi (SS) strain embryos and a putative founder animal was identified harboring an 18-bp deletion mutation (Rn5, chr10:99,084,780–99,084,797). This founder was back-crossed to the parental SS strain and a SS-*Kcnj16*^{em1Mcwi} ($SS^{Kcnj16-/-}$) breeding colony was established.

Dietary protocol and animal handling. At 8–9 weeks of age, the salt content of the chow was either maintained at 0.4% in the group fed a normal diet or increased to 4.0% NaCl (Dyets, Inc.; D113756), and the rats were maintained on these diets for up to 5 weeks. For experiments with high K^+ content, the final K^+ concentration was 1.41% (2% KCl was added to a base diet containing 0.36% of total K^+ concentration). For the survival experiments under high-salt conditions drinking water was provided ad libitum and supplemented with benzamil (15 mg/l), HCTZ (75 mg/l), or furosemide (in low 15 mg/l or high 150 mg/l concentrations). Urine samples were collected for 24 hours in metabolic cages to measure albuminuria, creatinine, and electrolytes. Blood samples were collected from the abdominal aorta for the measurement of plasma creatinine, BUN, and electrolytes concentrations before the final collection of tissues under anesthesia. Left kidneys were removed, formalin fixed, paraffin embedded, and then sections were stained with Masson's trichrome for quantification of kidney injury. The right kidneys were removed and used for electrophysiological and Western blotting analyses.

Blood pressure, renal function, and urine/serum biochemistry. At 8–9 weeks of age, rats were placed in metabolic cages (40615; Laboratory Products) to acclimate for 24 hours, followed by a 24-hour urine collection. Urine volume, Na^+, K^+, Mg^{2+}, creatinine, protein, and microalbumin were measured as described previously (54). Following urine collection, designated rats were anesthetized with 2%–3 % (vol/vol) isoflurane and a blood pressure transmitter (PA-C40; DSI) was surgically implanted subcutaneously, with the catheter tip secured in the abdominal aorta via the femoral artery. After a 3-day recovery period, blood pressure and heart rate were measured with a DSI system in conscious, freely moving male SS and $SS^{Kcnj16-/-}$ rats under different diet protocols, similar to those described previously (55, 56). Urine measurements were taken weekly during the high-salt challenge; in this case, Na^+, K^+, Cl^-, and Ca^{2+} electrolytes were measured with radiometric assay (ABL800 FLEX, Radiometer America Inc.). At the completion of the study, rats were anesthetized with 2%–3% (vol/vol) isoflurane and surgically prepared for a kidney flush and arterial blood collection. Blood electrolyte levels were immediately analyzed using the ABL800 FLEX blood gas analyzer.

The percentage of the electrolytes filtered by the kidney that was excreted in the urine was measured in terms of plasma and urine concentrations using following equations: FE (Na, K)(%) = ([Na, K] urine

to creatinine ratio/[Na, K] plasma to creatinine ratio) × 100, or FE (Mg)(%) = ([Mg] urine to creatinine ratio/0.7 × (Mg) plasma to creatinine ratio) × 100.

For aldosterone level analysis collected blood samples were centrifuged (6,000 *g*, 10 minutes), and then plasma was analyzed with Aldosterone RIA kits (MP Biomedicals) as previously reported (57).

Measurement of GFR in conscious rats. The GFR was measured in unrestrained conscious rats using a high-throughput method featuring detection of fluorescent FITC-labeled inulin (TdB Consultancy AB) clearance from blood. The method was adapted for rats from a protocol previously described for mice by Rieg (58). Predialyzed 20 mg/ml of FITC-inulin solution in saline (2 μl of 2% solution per 1 g of body weight) was administered by a bolus tail vein injection to rats briefly anesthetized with isoflurane. Immediately after the injection anesthesia was discontinued, and the animals were allowed to recover consciousness. Then, 10 μl of blood was collected 3, 5, 8, 16, 25, 40, 60, 80, 100, and 120 minutes after the injection by tail bleed. Next, plasma was separated, and inulin clearance was quantified by FITC intensity. Fluorescence measurements were performed using a NanoDrop 3300 Fluorospectrometer (Thermo Fisher Scientific). GFR was then calculated from the observed decrease in FITC fluorescence using a 2-compartment model (the initial fast decay representing the redistribution of FITC-inulin from the intravascular compartment to the extracellular fluid, and the slower phase reflecting clearance from plasma). The GFR curve was approximated with a bi-exponential decay function using OriginPro 9.0 (OriginLab) software, and GFR values in ml/min normalized to body weight were obtained from the fitting parameters using a previously described equation (58).

Western blotting and mRNA analysis. Kidney cortical lysates were prepared as follows (36). The SS or $SS^{Kcnj16-/-}$ rat kidneys were flushed with PBS in an anesthetized animal, excised and cut in 1- to 2-mm slices under a binocular microscope with ×6 magnification. The approximate apical kidney cortex sections were carved and then diced into small pieces with a razor blade. Samples were pulse sonicated in GLB with a protease inhibitor cocktail (Roche) for 10 seconds and spin cleared at 10,000 *g* for 10 minutes. The resulting supernatant was subjected to PAGE, transferred onto nitrocellulose membrane (Millipore) for probing with antibodies, and subsequently visualized by enhanced chemiluminescence (ECL; Amersham Biosciences). See complete unedited blots in the supplemental material.

For real-time PCR (RT-PCR) analysis tissue was collected from SS rats maintained on 0.4% or 4% NaCl diet. The kidney cortex was snap-frozen in liquid nitrogen and stored at −80°C. Total RNA was extracted using TRIzol reagent (ThermoFisher Scientific). The quality of each sample was assessed using an Agilent 2100 BioAnalzyer and quantity determined by spectrophotometry (Nanodrop). Two micrograms of total RNA was reverse transcribed by random hexamer primers into cDNA (Thermo Fisher Scientific RevertAid First-Strand cDNA synthesis kit) and real-time PCR analysis was performed using 8 to 10 ng total RNA with SYBR Green chemistry on an ABI Prism 7900HT (Applied Biosystems) as previously described (59). Primer sequences are given in the supplemental data.

Histological and IHC analysis. Kidneys were harvested for histological and IHC analysis using methods described previously (36). Kidney sections were cut at 4 μm, dried, and deparaffinized for subsequent labeling by streptavidin-biotin immunohistochemistry. After deparaffinization, slides were treated with a citrate buffer (pH 6) for a total of 35 minutes. Slides were incubated with peroxidase block (Dako), avidin block (Vector Laboratories), biotin block (Vector Laboratories), and serum-free protein block (Dako).

Tissue sections were incubated for 90 minutes in 1:500 dilutions of rabbit polyclonal antibody against $K_{ir}5.1$ and in 1:50 dilutions of goat polyclonal antibody against $K_{ir}4.1$ (ab74130 and ab105102, respectively, Abcam). Secondary detection was performed with anti-goat or anti-rabbit biotinylated IgG (BioCARE followed by streptavidin-horseradish peroxidase (BioCARE) and visualized with diaminobenzidine (Dako). All slides were counterstained with Mayer's hematoxylin (Dako), dehydrated, and mounted with permanent mounting medium (Sakura).

For double immunostaining images, kidney sections (4 μm) were labeled with rabbit anti-$K_{ir}5.1$ (SAB4501636, Sigma-Aldrich) and AQP2 (sc-28629, Santa Cruz Biotechnology) antibodies. Binding was revealed with Alexa Fluor 488 or 633 conjugated with goat anti-rabbit biotinylated IgG (Molecular Probes). Immunostaining was performed in tissues from at least 4 different kidneys. All tissue sections were examined by TCS SP5 confocal laser-scanning microscopy (Leica Microsystems).

For the kidney damage analysis, the tissue was stained with Masson's trichrome. Scoring of glomerular injury (average of 80 glomeruli quantified per kidney) was conducted blindly by at least 2 independent investigators according to previously published protocols (60). In brief, each visible glomerulus from a rep-

resentative kidney slice was scored from 0 (no injury) to 4 (nonfunctional, sclerotized) and an average score was calculated for each kidney. A protein cast analysis was performed with a color thresholding method using MetaMorph (Molecular Devices) software. Results are reported as a percentage of the casts in the total medullary area.

Deconvolution algorithm–based processing of immunostained images (Figure 1A and Figure 4, C and D) was used for the quantification of protein abundance and distribution (ImageJ v1.47, NIH; Color deconvolution module). Briefly, the signal representing protein staining was deconvoluted from recorded images by H&E DAB or similar filter. Color intensity for the region of interest (single tubule) was calculated by ROI Manager module (ImageJ v1.47). Protein distribution on apical/basolateral sides was estimated by comparison of the corresponding region of interest for each tubule.

Isolation of cortical collecting ducts. Patch-clamp electrophysiology was used to assess the activity of K_{ir} channels in the isolated rat CCD. CCDs were isolated from SS and $SS^{Kcnj16-/-}$ rats, as described previously (18). Kidneys were cut into thin slices (<1 mm) and then incubated in physiologic saline solution (pH 7.4) containing 0.8 mg/ml collagenase I (Alfa Aesar, J62406) and 5 mg/ml dispase II (Roche, 04942078001). Then CCDs were mechanically isolated from slices by microdissection using forceps under a stereomicroscope and attached to a cover glass chips coated with poly-L-lysine (Sigma-Aldrich).

Electrophysiology. Single-channel data were acquired and subsequently analyzed with Axopatch 200B or 700B amplifiers (Molecular Devices) interfaced via a Digidata 1440A to a PC running the pClamp 10.2 suite of software (Molecular Devices). The currents acquired with an Axopatch 200B amplifier were filtered with an 8-pole, low-pass Bessel filter LPF-8 (Warner Inst.) at 0.3 kHz. The pipette was pulled with a horizontal puller (Sutter P-97; Sutter Inst.). The resistance of the pipette in the corresponding bath medium was 7–12 MΩ. The single-channel activity of $K_{ir}4.1/5.1$ and $K_{ir}4.1$ channels in CCD cells was determined in cell-attached patches on the basolateral membrane made under voltage-clamp conditions. Bath and pipette solutions were (in mM) 150 NaCl, 5 KCl, 1 $CaCl_2$, 2 $MgCl_2$, 5 glucose, and 10 HEPES (pH 7.35) and 150 KCl, 2 $MgCl_2$, and 10 HEPES (pH 7.35), respectively. Current-voltage (I-V) relationships were obtained by monitoring channel activity at applied pipette voltages (−Vp) from −120 to +20 mV with a step of 20 mV for at least 180 seconds. The channel events were analyzed by Clampfit 10.2 software "single-channel search" in Analyze function in conjunction with OriginPro 9.0. A 50% threshold cross method was utilized to determine valid channel openings. All events were carefully checked visually before being accepted. Single-channel unitary current (i) was determined from the best-fit Gaussian distribution of amplitude histograms. Activity was analyzed as $NP_o = I/i$, where I is the mean total current in a patch and i is unitary current at this voltage. P_o was calculated by normalizing NP_o for the total number of estimated channels (N) in the patch.

Statistics. Data were compared using 1-way ANOVA followed by a Bonferroni or Tukey comparison tests of means. Data are represented as box-and-whisker plots that indicate mean value, standard error (box), and standard deviation (whisker). Differences were considered statistically significant at P less than 0.05.

Study approval. All animal experiments were conducted in accordance with the NIH Guide for the Care and Use of Laboratory Animals following protocol review and approval by the Medical College of Wisconsin Institutional Animal Care and Use Committee.

Author contributions

AS and O. Palygin conceptualized the study. O. Palygin, VL, DVI, TSP, and AS conducted the investigation. HJJ and AMG created rat model used in the study. O. Pochynyuk and MRH contributed to the interpretation of data. O. Palygin and AS wrote the original draft of the manuscript. O. Palygin, VL, DVI, O. Pochynyuk, HJJ, AMG, MRH, and AS reviewed and edited the manuscript. AS supervised the study.

Acknowledgments

We would like to thank Jessica L. Barnett, Oleh Prudnikov, Christine Nguyen, Jennifer M Connell, and Chun Yang for experimental help and analysis; Paula North and Christine Duris for histology and immunohistochemistry experiments and their interpretation; David L. Mattson, Lisa Henderson, and Camille Torres for help with biochemical assays; and Andrey Ilatovskiy for development of software used in GFR measurements. David H. Ellison (Oregon Health & Science University, Portland) and Pablo Ortiz (Henry Ford Hospital, Detroit) are greatly appreciated for providing antibodies. This research was supported by the NIH grants HL135749, HL10880, HL122662 (to A.S.), HL122358 (to M.H.), HL101681 (to H.J. and

A.G.), OD008396 (A.G.); MCW NRC/AHW pilot grant 9520217 (to O. Palygin and M.H.); and American Heart Association grants 16EIA26720006 (to A.S.) and 17SDG33660149 (to O. Palygin).

Address correspondence to: Alexander Staruschenko, Department of Physiology, Medical College of Wisconsin, 8701 Watertown Plank Road, Milwaukee, Wisconsin 53226, USA. Phone: 414.955.8475; Email: staruschenko@mcw.edu.

HJJ's present address is: HudsonAlpha Institute for Biotechnology, 601 Genome Way, Huntsville, Alabama, USA.

TSP's present address is: Hypertension and Vascular Research Division, Henry Ford Health System, Detroit, Michigan, USA.

1. Kotchen TA, Cowley AW, Frohlich ED. Salt in health and disease--a delicate balance. *N Engl J Med*. 2013;368(13):1229–1237.
2. Mente A, et al. Association of urinary sodium and potassium excretion with blood pressure. *N Engl J Med*. 2014;371(7):601–611.
3. O'Donnell M, et al. Urinary sodium and potassium excretion, mortality, and cardiovascular events. *N Engl J Med*. 2014;371(7):612–623.
4. Mente A, Irvine EJ, Honey RJ, Logan AG. Urinary potassium is a clinically useful test to detect a poor quality diet. *J Nutr*. 2009;139(4):743–749.
5. Chang HY, et al. Effect of potassium-enriched salt on cardiovascular mortality and medical expenses of elderly men. *Am J Clin Nutr*. 2006;83(6):1289–1296.
6. Gumz ML, Rabinowitz L, Wingo CS. An integrated view of potassium homeostasis. *N Engl J Med*. 2015;373(1):60–72.
7. Palmer BF. Regulation of potassium homeostasis. *Clin J Am Soc Nephrol*. 2015;10(6):1050–1060.
8. Terker AS, et al. Potassium modulates electrolyte balance and blood pressure through effects on distal cell voltage and chloride. *Cell Metab*. 2015;21(1):39–50.
9. Palygin O, Pochynyuk O, Staruschenko A. Role and mechanisms of regulation of the basolateral Kir 4.1/Kir 5.1K(+) channels in the distal tubules. *Acta Physiol (Oxf)*. 2017;219(1):260–273.
10. Wang WH. Basolateral Kir4.1 activity in the distal convoluted tubule regulates K secretion by determining NaCl cotransporter activity. *Curr Opin Nephrol Hypertens*. 2016;25(5):429–435.
11. Cuevas CA, et al. Potassium sensing by renal distal tubules requires Kir4.1. *J Am Soc Nephrol*. 2017;28(6):1814–1825.
12. Pessia M, Tucker SJ, Lee K, Bond CT, Adelman JP. Subunit positional effects revealed by novel heteromeric inwardly rectifying K^+ channels. *EMBO J*. 1996;15(12):2980–2987.
13. Pessia M, Imbrici P, D'Adamo MC, Salvatore L, Tucker SJ. Differential pH sensitivity of Kir4.1 and Kir4.2 potassium channels and their modulation by heteropolymerisation with Kir5.1. *J Physiol (Lond)*. 2001;532(Pt 2):359–367.
14. D'Adamo MC, Shang L, Imbrici P, Brown SD, Pessia M, Tucker SJ. Genetic inactivation of Kcnj16 identifies Kir5.1 as an important determinant of neuronal PCO2/pH sensitivity. *J Biol Chem*. 2011;286(1):192–198.
15. Tucker SJ, Imbrici P, Salvatore L, D'Adamo MC, Pessia M. pH dependence of the inwardly rectifying potassium channel, Kir5.1, and localization in renal tubular epithelia. *J Biol Chem*. 2000;275(22):16404–16407.
16. Lourdel S, et al. An inward rectifier K(+) channel at the basolateral membrane of the mouse distal convoluted tubule: similarities with Kir4-Kir5.1 heteromeric channels. *J Physiol (Lond)*. 2002;538(Pt 2):391–404.
17. Lachheb S, et al. Kir4.1/Kir5.1 channel forms the major K^+ channel in the basolateral membrane of mouse renal collecting duct principal cells. *Am J Physiol Renal Physiol*. 2008;294(6):F1398–F1407.
18. Zaika OL, Mamenko M, Palygin O, Boukelmoune N, Staruschenko A, Pochynyuk O. Direct inhibition of basolateral Kir4.1/5.1 and Kir4.1 channels in the cortical collecting duct by dopamine. *Am J Physiol Renal Physiol*. 2013;305(9):F1277–F1287.
19. Zaika O, Palygin O, Tomilin V, Mamenko M, Staruschenko A, Pochynyuk O. Insulin and IGF-1 activate Kir4.1/5.1 channels in cortical collecting duct principal cells to control basolateral membrane voltage. *Am J Physiol Renal Physiol*. 2016;310(4):F311–F321.
20. Reichold M, et al. KCNJ10 gene mutations causing EAST syndrome (epilepsy, ataxia, sensorineural deafness, and tubulopathy) disrupt channel function. *Proc Natl Acad Sci U S A*. 2010;107(32):14490–14495.
21. Bockenhauer D, et al. Epilepsy, ataxia, sensorineural deafness, tubulopathy, and KCNJ10 mutations. *N Engl J Med*. 2009;360(19):1960–1970.
22. Scholl UI, et al. Seizures, sensorineural deafness, ataxia, mental retardation, and electrolyte imbalance (SeSAME syndrome) caused by mutations in KCNJ10. *Proc Natl Acad Sci U S A*. 2009;106(14):5842–5847.
23. Zhang C, et al. KCNJ10 determines the expression of the apical Na-Cl cotransporter (NCC) in the early distal convoluted tubule (DCT1). *Proc Natl Acad Sci U S A*. 2014;111(32):11864–11869.
24. Su XT, Zhang C, Wang L, Gu R, Lin DH, Wang WH. Disruption of KCNJ10 (Kir4.1) stimulates the expression of ENaC in the collecting duct. *Am J Physiol Renal Physiol*. 2016;310(10):F985–F993.
25. Paulais M, et al. Renal phenotype in mice lacking the Kir5.1 (Kcnj16) K^+ channel subunit contrasts with that observed in SeSAME/EAST syndrome. *Proc Natl Acad Sci U S A*. 2011;108(25):10361–10366.
26. Juang JM, et al. Disease-targeted sequencing of ion channel genes identifies de novo mutations in patients with non-familial Brugada syndrome. *Sci Rep*. 2014;4:6733.

27. Demirkan A, et al. Insight in genome-wide association of metabolite quantitative traits by exome sequence analyses. *PLoS Genet*. 2015;11(1):e1004835.
28. Kompatscher A, et al. Loss of transcriptional activation of the potassium channel Kir5.1 by HNF1β drives autosomal dominant tubulointerstitial kidney disease [published online ahead pf print May 31, 2017]. *Kidney Int*. https://doi.org/10.1016/j.kint.2017.03.034.
29. Tobian L. Salt and hypertension. Lessons from animal models that relate to human hypertension. *Hypertension*. 1991;17(1 Suppl):I52–I58.
30. Rapp JP. Dahl salt-susceptible and salt-resistant rats. A review. *Hypertension*. 1982;4(6):753–763.
31. Cowley AW. The genetic dissection of essential hypertension. *Nat Rev Genet*. 2006;7(11):829–840.
32. Geurts AM, et al. Knockout rats via embryo microinjection of zinc-finger nucleases. *Science*. 2009;325(5939):433.
33. Zhang C, Wang L, Su XT, Lin DH, Wang WH. KCNJ10 (Kir4.1) is expressed in the basolateral membrane of the cortical thick ascending limb. *Am J Physiol Renal Physiol*. 2015;308(11):F1288–F1296.
34. Rodan AR. Potassium: friend or foe? *Pediatr Nephrol*. 2017;32(7):1109–1121.
35. Ray PE, Suga S, Liu XH, Huang X, Johnson RJ. Chronic potassium depletion induces renal injury, salt sensitivity, and hypertension in young rats. *Kidney Int*. 2001;59(5):1850–1858.
36. Pavlov TS, et al. Deficiency of renal cortical EGF increases ENaC activity and contributes to salt-sensitive hypertension. *J Am Soc Nephrol*. 2013;24(7):1053–1062.
37. Kakizoe Y, et al. Aberrant ENaC activation in Dahl salt-sensitive rats. *J Hypertens*. 2009;27(8):1679–1689.
38. Pavlov TS, Staruschenko A. Involvement of ENaC in the development of salt-sensitive hypertension. *Am J Physiol Renal Physiol*. 2017;313(2):F135–F140.
39. Pochynyuk O, et al. Dietary Na^+ inhibits the open probability of the epithelial sodium channel in the kidney by enhancing apical P2Y2-receptor tone. *FASEB J*. 2010;24(6):2056–2065.
40. McDonough AA, Veiras LC, Guevara CA, Ralph DL. Cardiovascular benefits associated with higher dietary K(+) vs. lower dietary Na(+): evidence from population and mechanistic studies. *Am J Physiol Endocrinol Metab*. 2017;312(4):E348–E356.
41. Ellison DH, Terker AS, Gamba G. Potassium and its discontents: new insight, new treatments. *J Am Soc Nephrol*. 2016;27(4):981–989.
42. Cowley AW. Long-term control of arterial blood pressure. *Physiol Rev*. 1992;72(1):231–300.
43. Staruschenko A. Regulation of transport in the connecting tubule and cortical collecting duct. *Compr Physiol*. 2012;2(2):1541–1584.
44. Hall JE. Renal dysfunction, rather than nonrenal vascular dysfunction, mediates salt-induced hypertension. *Circulation*. 2016;133(9):894–906.
45. Feng D, et al. Increased expression of NAD(P)H oxidase subunit p67(phox) in the renal medulla contributes to excess oxidative stress and salt-sensitive hypertension. *Cell Metab*. 2012;15(2):201–208.
46. Geurts AM, et al. Maternal diet during gestation and lactation modifies the severity of salt-induced hypertension and renal injury in Dahl salt-sensitive rats. *Hypertension*. 2015;65(2):447–455.
47. Penton D, Czogalla J, Loffing J. Dietary potassium and the renal control of salt balance and blood pressure. *Pflugers Arch*. 2015;467(3):513–530.
48. Moore TJ, Conlin PR, Ard J, Svetkey LP. DASH (Dietary Approaches to Stop Hypertension) diet is effective treatment for stage 1 isolated systolic hypertension. *Hypertension*. 2001;38(2):155–158.
49. Saneei P, Salehi-Abargouei A, Esmaillzadeh A, Azadbakht L. Influence of Dietary Approaches to Stop Hypertension (DASH) diet on blood pressure: a systematic review and meta-analysis on randomized controlled trials. *Nutr Metab Cardiovasc Dis*. 2014;24(12):1253–1261.
50. Veiras LC, Han J, Ralph DL, McDonough AA. Potassium supplementation prevents sodium chloride cotransporter stimulation during angiotensin ii hypertension. *Hypertension*. 2016;68(4):904–912.
51. Bazúa-Valenti S, et al. The effect of WNK4 on the Na^+-Cl^- cotransporter is modulated by intracellular chloride. *J Am Soc Nephrol*. 2015;26(8):1781–1786.
52. Penton D, et al. Extracellular K(+) rapidly controls NaCl cotransporter phosphorylation in the native distal convoluted tubule by Cl(-) -dependent and independent mechanisms. *J Physiol (Lond)*. 2016;594(21):6319–6331.
53. Geurts AM, et al. Generation of gene-specific mutated rats using zinc-finger nucleases. *Methods Mol Biol*. 2010;597:211–225.
54. Moreno C, et al. Creation and characterization of a renin knockout rat. *Hypertension*. 2011;57(3):614–619.
55. Endres BT, et al. Mutation of Plekha7 attenuates salt-sensitive hypertension in the rat. *Proc Natl Acad Sci U S A*. 2014;111(35):12817–12822.
56. Pavlov TS, et al. Lack of effects of metformin and AICAR chronic infusion on the development of hypertension in Dahl salt-sensitive rats. *Front Physiol*. 2017;8:227.
57. Pavlov TS, Levchenko V, Ilatovskaya DV, Moreno C, Staruschenko A. Renal sodium transport in renin-deficient Dahl salt-sensitive rats. *J Renin Angiotensin Aldosterone Syst*. 2016;17(3):1470320316653858.
58. Rieg T. A High-throughput method for measurement of glomerular filtration rate in conscious mice. *J Vis Exp*. 2013;75(75):e50330.
59. Cowley AW, et al. Evidence of the importance of Nox4 in production of hypertension in Dahl salt-sensitive rats. *Hypertension*. 2016;67(2):440–450.
60. Raij L, Azar S, Keane W. Mesangial immune injury, hypertension, and progressive glomerular damage in Dahl rats. *Kidney Int*. 1984;26(2):137–143.